

Sensorless Control for a Switched Reluctance Wind Generator, Based on Current Slopes and Neural Networks

Estanislao Echenique, Juan Dixon, *Senior Member, IEEE*, Roberto Cárdenas, *Senior Member, IEEE*, and Ruben Peña, *Member, IEEE*

Abstract—In this paper, the analysis, design, and implementation of a novel rotor position estimator for the control of variable-speed switched reluctance generators (SRGs) are presented. The rotor position is obtained using the unsaturated instantaneous inductance. This unsaturated inductance is estimated calculating the slope of the phase current and using a reduced-size neural network (NN) whose inputs are the average current and the saturated inductance. The proposed estimator requires less processing time than traditional methods and can be fully implemented using a low-cost DSP with very few additional analog/digital components. The rotor position estimator presented in this paper can be applied to a wind energy conversion system where the SRG is used as a variable-speed generator. This application is currently being studied because the SRG has well-known advantages such as robustness, low manufacturing cost, and good size-to-power ratio. Simulation and experimental results are presented using a 2.5-kW 8/6-SRG prototype.

Index Terms—Neural networks (NNs), position control, wind power generation.

I. INTRODUCTION

LOW manufacturing cost, fault tolerance, high robustness, and high efficiency are well-known advantages of switched reluctance generators (SRGs). This machine has remarkable characteristics that enable it to be used as a variable-speed generator, specifically in a wind energy conversion system (WECS). Additionally, the SRG can generate electrical power in a wide speed range without requiring a gearbox [1]. Moreover, the SRG has a very good efficiency in the whole operating range.

The use of SRGs in wind energy applications has been studied for more than 20 years. However, control methods for WECS applications have been developed only recently. In [2],

a control system is presented for the operation of an SRG driven by a variable-speed wind turbine. The system interfaces with the ac grid using a pulsewidth-modulation (PWM) inverter. In [3], a variable-speed wind turbine is proposed using a small-power (800 W) SRG that is controlled using a maximum power point tracking algorithm. The generated power is dissipated in a resistive load. In [4], it is proposed to use an SRG operating as a support system in a WECS when the wind speed is low. In [5], an optimized design of the SRG for maximum output power is presented. In [6], a generating system based on a simple controller is proposed. The optimal firing angles are determined online. The SRG can operate feeding a three-phase ac stand-alone system [7], [8] or driving a flywheel for an energy storage and power smoothing system [9].

In the applications reported in [1]–[9], the SRG requires a position sensor for the commutation of the stator phases in synchronism with the rotor position. Position sensing not only means higher cost and additional complexity but also increases the vulnerability of electronic systems. In some applications, environmental conditions do not allow the use of encoders.

To avoid the use of a position encoder, it is necessary to use control algorithms that are able to estimate the position of the rotor. Recently, position sensorless control strategies for switched reluctance machines (SRMs) based on mathematical models of the system have been developed [10]. These sensorless methods do not require extra hardware (oscillators, sensing circuits, etc.), but they are not simple to implement, and they usually require fast and expensive processors to achieve the required processing speed.

The general principle for sensorless control methods relies on the magnetic characteristics of the SRM that vary with the rotor position. The measured variables are typically the phase voltages and the phase currents. The estimated variable is the inductance or the flux linkage. From them, the rotor position can be determined.

Neural networks (NN) and other modern control techniques have been used to construct a map between current, flux linkage, and rotor position, since they have an inherent capacity to model system nonlinearities, as is the case of the SRM [11]. These methods have demonstrated a satisfactory operation [12], [13], but they normally require a high processing capability. However, in [14], a remarkable reduction of the total number of neurons is obtained by inserting a preprocessor between flux linkage and current. The proposed control was implemented in

Manuscript received March 4, 2008; revised August 20, 2008. First published October 24, 2008; current version published February 27, 2009. This work was supported by Millennium Project P-04-048-F.

E. Echenique is with Systep Engineering and Design Company, Santiago 755-0171, Chile (e-mail: ejecheni@gmail.com).

J. Dixon is with the Department of Electrical Engineering, Pontificia Universidad Católica de Chile, Santiago 782-0436, Chile (e-mail: jdixon@ing.puc.cl).

R. Cárdenas is with the Department of Electrical Engineering, Universidad de Magallanes, Punta Arenas 621-0427, Chile (e-mail: rcd@iee.org).

R. Peña is with the Department of Electrical Engineering, Universidad de Concepción, Concepción 407-0386, Chile (e-mail: rupena@udec.cl).

Color versions of one or more of the figures in this paper are available online at <http://ieeexplore.ieee.org>.

Digital Object Identifier 10.1109/TIE.2008.2005940

a two-phase SRM and produces an appropriate performance, without requiring analog integrators for the experimental implementation.

Sensorless methods based on the estimation of the flux linkage have well-known problems at low rotational speeds, because these methods are strongly affected by the variation of the phase resistance. Usually, analog integrators are used, as in [12], but they are not fully reliable because the integrator behavior changes with time. There are no publications that report the use of the instantaneous inductance as the input of an NN. The advantage of a sensorless method based on the instantaneous inductance derives from the fact that the estimation of this parameter is not affected by variations on the phase resistance [15].

The method proposed in [16] can operate at any rotational speed, but at low speeds, it requires the injection of exploratory signals in an inactive phase. In [17], another sensorless method is proposed that also reduces the acoustic noise produced by the SRM. Nevertheless, this method is suitable only at single-pulse mode. In [18], a position estimator is presented using a sliding-mode observer, but the computational requirements are very high, and the proposed state observer does not have a good performance in a strongly nonlinear system as an SRG.

Finally, sensorless control of SRGs has been reported for high-speed operation in [19] and [20], but again, it is assumed that the machine is controlled using single-pulse mode. There are no publications related to sensorless control of SRGs, operating in a wide speed range, from low to high mechanical speeds, under a scheme of chopping control of the phase currents. In this paper, the method proposed in [15] for the control of an SRM has been revised, modified, and applied to an SRG. The method is based on the fact that the current slope is a function of the dc input voltage and the machine phase inductance. The contribution of the sensorless method proposed in this paper consists in calculating the current slopes by the least mean squares (LMS) method [21] and the use of an NN to approximate the function that relates saturated inductance and current to a phase unsaturated inductance. The commutation instants are determined online from the instantaneous inductance, not by the rotor position, as traditionally reported.

Experimental results are presented in this paper. An experimental system based on a four-phase 2.5-kW 8/6 SRG is used to validate the proposed sensorless method.

II. ANALYSIS OF SRG OPERATION

The voltage for each phase of the SRG is given by

$$v_{ph} = Ri + \frac{d\lambda}{dt} = Ri + L\frac{di}{dt} + \omega_m i \frac{dL}{d\theta} \quad (1)$$

where λ is the flux linkage, i is the phase current, R is the phase resistance, L is the inductance, ω_m is the rotor angular velocity, and θ is the rotor position. If magnetic saturation is ignored, the instantaneous electromagnetic torque is given by

$$T_e = \frac{1}{2} i^2 \frac{dL}{d\theta}. \quad (2)$$

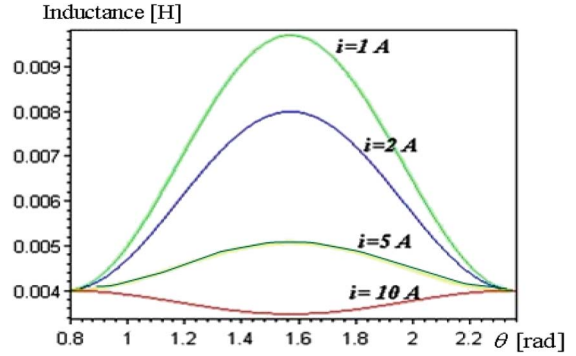


Fig. 1. Inductance profile as a function of current and rotor position in an SRM.

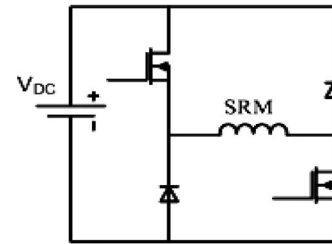


Fig. 2. Classical asymmetric inverter for SRMs.

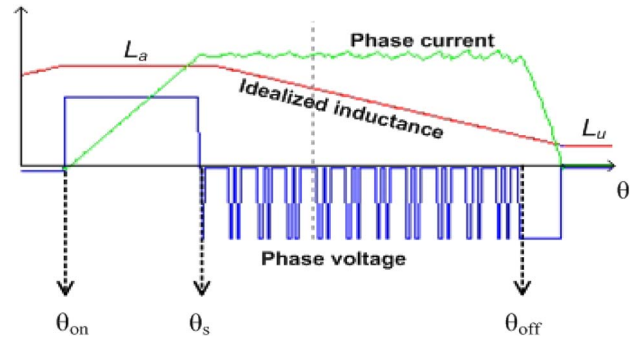


Fig. 3. Typical waveforms of a soft-chopping current-controlled SRG.

Generation torque is produced when the phase winding is energized during the negative slope of the phase inductance variation, i.e., after the aligned position. Fig. 1 shows the relation between inductance and rotor position for different phase currents. The inductance gives useful information about the rotor position except when high currents are applied.

A. Current Regulation in an SRG

Fig. 2 shows one phase of a classical asymmetric configuration for SRM. Considering the SRG near or in the alignment position, and assuming a particular speed, when both switches of Fig. 2 are turned on in θ_{on} (see Fig. 3), the voltage applied in the winding is $+V_{dc}$. After θ_{on} , the current increases until both switches are turned off in θ_{off} . The current normally reaches a reference level imposed by the control. When both switches are off, the voltage applied in the phase is $-V_{dc}$, and the winding supplies energy back to the voltage source. In order to maintain a constant current during the negative-slope region, at least one

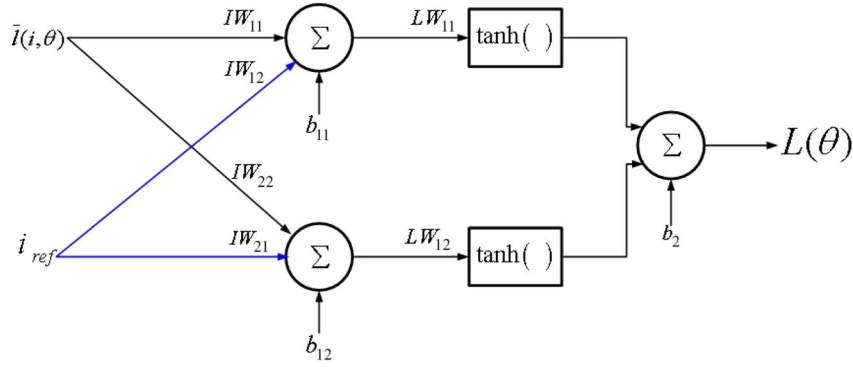


Fig. 4. Diagram of the proposed NN.

of the switches is turned on and off, depending on the current controller output. If only one of them is turn off while the other is chopped, then the SRG is operated in soft chopping, as shown in Fig. 3. On the other hand, if both switches are simultaneously turned on and off, then the SRG is operated in hard chopping. For generation, the phase voltage is switched on/off, to regulate the current, until the phase inductance reaches the minimum value, L_u (unaligned position). At this point, the phase current is forced to zero ($\theta = \theta_{\text{off}}$) to avoid the production of motoring torque in the machine.

III. PROPOSED INDUCTANCE ESTIMATOR

If the average phase current is assumed to be constant between consecutive commutations and the frequency of the PWM signal is high compared with the rotational frequency of the machine, then the inductance could be estimated by [15]

$$\frac{2V_{\text{DC}}}{\frac{di}{dt_{\uparrow}} - \frac{di}{dt_{\downarrow}}} = l(i, \theta), \quad \text{for hard switching} \quad (3)$$

$$\frac{V_{\text{DC}}}{\frac{di}{dt_0} - \frac{di}{dt_1}} = l(i, \theta), \quad \text{for soft switching} \quad (4)$$

where di/dt_{\uparrow} and di/dt_{\downarrow} are the positive and negative slopes of a given phase current, respectively. Therefore, using a numerical differentiation of the phase current and assuming that the voltage applied is known, it is possible to have an online determination of the machine inductance. The instantaneous current slopes are calculated using the LMS method [21] in a simplified and recursive version that reduces the processing time and, in addition, is less susceptible to noise. In each state of the PWM signal, the current is sampled at a fixed rate. When the commutation occurs, the DSP calculates the current slope needed to determine the instantaneous inductance. Because the phase current is sampled at a fixed rate, the current slope is given by

$$m = \frac{z_N}{N(N^2 - 1)} \quad (5)$$

where

$$z_N = z_{N-1} + \sum_{i=1}^{N-1} i_i - (N-1)i_N \quad (6)$$

where N is the number of samples in a state of commutation, i_i is the i th sampled current, and i_N is the last current sample. Moreover, $z_0 = 0$, and the term $[N(N^2 - 1)]^{-1}$ can be obtained from a lookup table (no more than 16 terms), avoiding a mathematical division that requires several instructions in a fixed-point DSP. A total of four additions and one multiplication is required in each current sample. With this method, it is possible to estimate the inductance at any rotational speed. In this paper, the method has been experimentally demonstrated for a speed range between 0 and 1500 rpm.

Another contribution of the developed method consists in the use of an NN to approximate the function that relates saturated inductance and current to an unsaturated inductance. This is necessary because the machine inductance gives ambiguous information when the machine is saturated and the phase current is high, as shown in Fig. 1.

A classic configuration of a multilayer NN is used in this paper to approximate a nonlinear function. The NN contains only two layers and three neurons (see Fig. 4). The sigmoidal and hyperbolic tangent (\tanh) functions are commonly used in power electronic systems [22], and they are considered in this paper. The inputs to the proposed NN are the reference current and the estimated inductance $l(i, \theta)$. There is only one output, and it is the unsaturated inductance $L(\theta)$. The output is dependent on the rotor position only. Offline training of the NN is achieved by using the backpropagation algorithm of one of the MATLAB toolboxes. The data used in the training stage are experimentally obtained from the prototype discussed in Section VI. In the experimental setup, the unsaturated inductance and rotor angle were obtained using an inductance meter and a rotor position encoder of 2500 pulses per revolution.

The optimization procedure proposed in [6] for current-controlled SRGs is applied in this paper. The method discussed in [6] can be explained using Fig. 5. In order to optimize the use of the generating torque area, corresponding to the negative-slope region of the unsaturated inductance, the machine phase switch has to be turned on when the rotor position angle is θ_{on_i+1} and the instantaneous inductance is $L\theta_{\text{on}_i+1}$ (see Fig. 5). On the other hand, to avoid motoring torque, the phase switch is turned off when the instantaneous inductance is $L\theta_{\text{off}_i}$. In this case, the phase current i_A reaches zero when the rotor pole is fully unaligned with the stator pole.

The novelty of the work is to determine when to turn on and off a particular phase switch, using the instantaneous

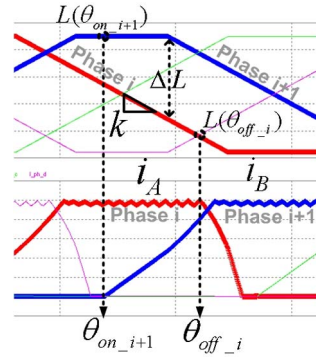


Fig. 5. 8/6-SRG typical waveforms considering the overlapping of two neighboring phases.

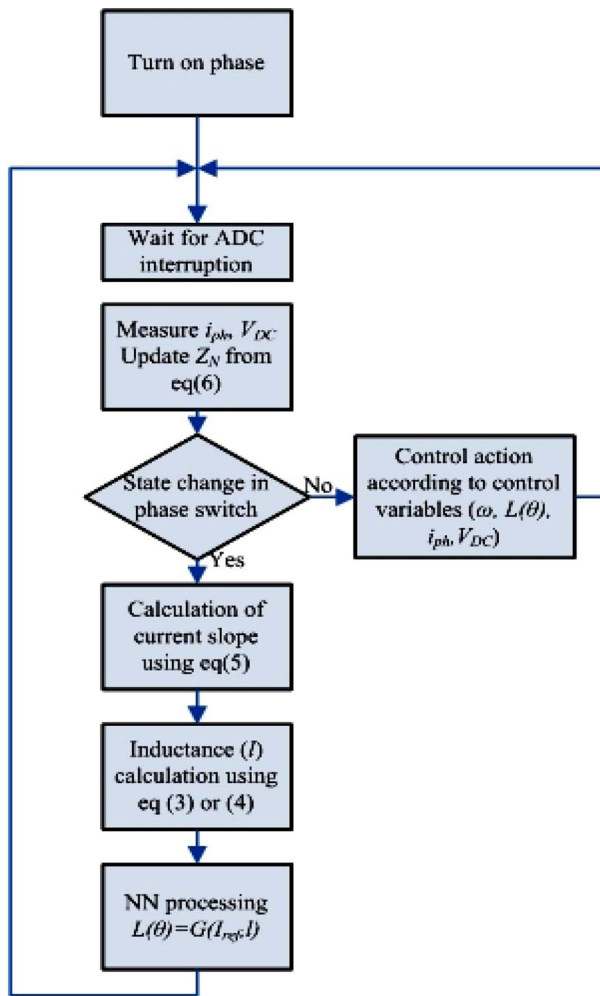


Fig. 6. Flowchart of the inductance estimator.

inductance, not the overlapping angles. Therefore, the proposed estimation algorithm uses a different approach compared to traditional methods. It does not determine directly the absolute rotor position, but instead the value of the unsaturated inductance, which provides the same information as the rotor angle but requires less processing time.

In Fig. 6, a flowchart of the inductance estimation procedure proposed in this paper is presented. The algorithm shown in Fig. 6 is slightly changed during the starting-up stage of the

sensorless algorithm and when the SRG is generating. However, the inductance estimation procedure is identical in all the cases.

For starting up, a small current is applied in one phase of the SRG for about three electric cycles to determine the speed and the instant where the generation begins. During generation, additional control actions are required to determine, for example, which of the four phases has to be energized, when the next phase has to be excited, the turn-off instant of the actual phase, etc.

For the experimental system used in this paper, the SRG operates initially excited by an external dc source V_{ext} and fed by a power inverter of six switches and diodes (see Fig. 7). Once it has entered the generation regime, the voltage generated in the load will be higher than V_{ext} , and then, the external source is no longer required.

IV. PROPOSED CONTROL SYSTEM

The demanded reference current i_{ref} in Fig. 8 is obtained from a PI controller which regulates the load voltage. The error between i_{ref} and the actual phase current is processed by another PI controller which generates a signal, corresponding to a duty cycle D , used for the pulse generator. The turn-on and turn-off signals of the insulated-gate bipolar transistors (IGBTs) are obtained from a pulse generator that uses as inputs the duty cycle signal from the current control loop, the instantaneous linear inductance of the machine, and the L_{on} and L_{off} inductances. There are other control strategies that are more suitable for the control of variable-speed WECSs that control the generated power rather than the voltage, as reported in [2], but they are considered outside the scope of this paper. However, the estimation algorithm proposed in this paper can be implemented in any kind of inverter topology and control scheme.

In variable-speed wind generation, the optimal power that can be extracted from the wind is given by

$$P_{opt} = k_{opt} \omega_m^3 \quad (7)$$

where P_{opt} is the optimal power and k_{opt} is a constant that depends on the blade aerodynamic, gearbox ratio, and wind turbine parameters [2]. From (7) and balancing the load with the generation, it is possible to determine the dc-link voltage demand for a given SRG speed. This voltage is obtained by

$$V_{DC}^* = f(\omega_m) = \sqrt{R_L k_{opt} \omega_m^3}. \quad (8)$$

The load voltage is regulated in order to maintain a sufficiently high voltage value to ensure operation in current regulation mode. Therefore, the SRG never operates in single-pulse mode achieving the operation of the proposed sensorless algorithm in a wide range of mechanical speeds.

SRM torque ripple reduction is simpler to achieve when the machine is operating in chopping control of the phase current instead of single-pulse mode [23], [24]. Moreover, torque smoothness is essential in many direct-drive applications, which require high torque at low speeds. Current regulation is normally used in a WECS [25].

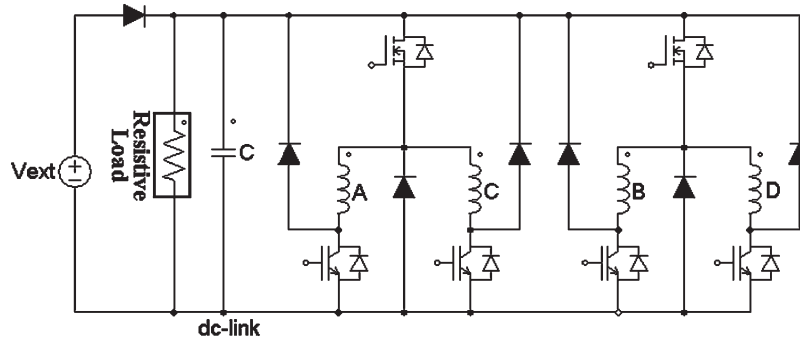


Fig. 7. Inverter configuration.

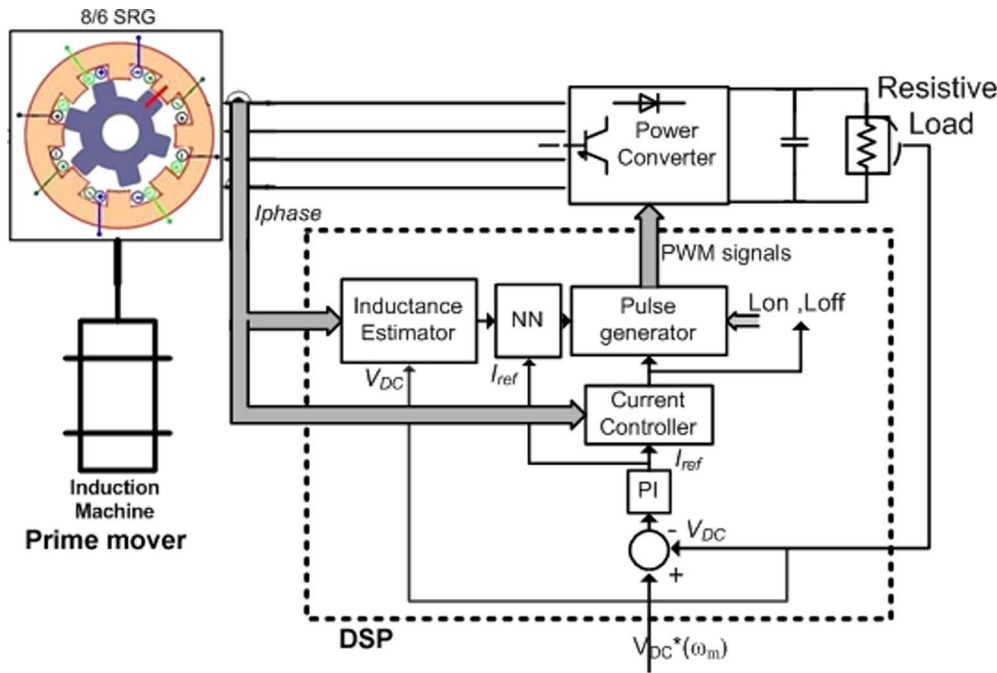


Fig. 8. Control system implemented.

V. SIMULATION RESULTS

Because most of the modern SRGs operate considering substantial saturation of the machine iron, the nonlinear characteristic effect of saturation is considered for proper simulation of the machine.

In Fig. 9, simulation results of the inductance estimator are presented for different phase currents. The waveform curve covers both regions, motoring and generating, because a constant current has been applied to the machine phase.

For the application discussed in this paper, the estimator operates only in the negative-slope region. It is clearly observed that the estimated inductance waveform is very close to that of the saturated inductance. The ripple in both waveforms is due to the 5-kHz PWM frequency. In the aligned position, the estimated inductance reduces its peak value as the phase current increases, because of iron saturation. Therefore, the NN is used to obtain the unsaturated instantaneous inductance, using as inputs i_{ref} and the estimated inductance.

In Fig. 10, waveforms of reference inductance ($L(\theta)_{ref}$) and the NN output ($L(\theta)_{NN}$) are presented. Additionally, the absolute error between both waveforms that represents the error in

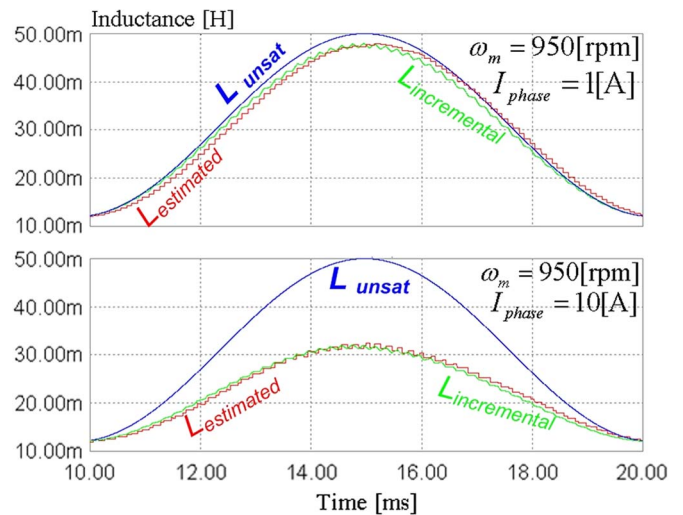


Fig. 9. Waveforms of estimated, unsaturated, and incremental inductances for 1 and 10 A.

inductance estimation is shown. The NN adjusts satisfactorily to the reference inductance, in any rotor position. A greater error in the region of alignment is observed, but in a generation

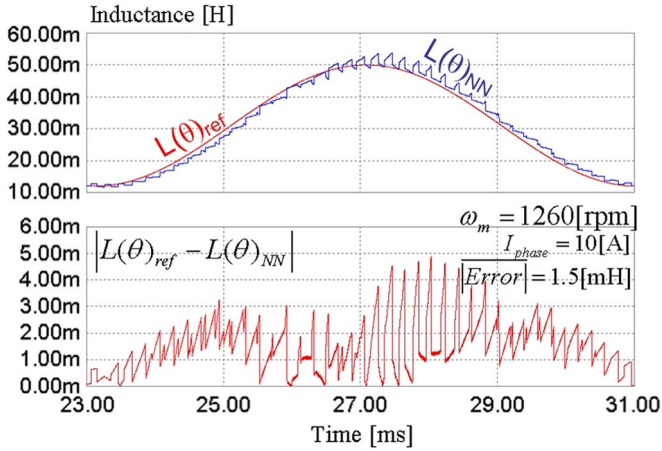


Fig. 10. Simulated waveforms of estimated-inductance and absolute-inductance error using an NN.

scheme and according to the control proposed in this paper, it is more important to estimate the inductance, with low error, in the region of pole misalignment. A maximum error of ± 4.9 mH is observed at a speed of 1260 rpm and a current of 10 A. This means, in terms of rotor position, an error of $\pm 2.7^\circ$ (mechanical degrees). This is because, in the negative-slope region

$$\left| \frac{\Delta L}{\Delta \theta} \right| \approx 1.809 \left[\frac{\text{mH}}{\text{degrees}} \right]. \quad (9)$$

The performance of the inductance estimator is not affected by speed disturbances because the instantaneous inductance does not depend on speed. This is further corroborated by the experimental results.

VI. EXPERIMENTAL RESULTS

The proposed sensorless algorithm (i.e., the inductance estimator and the NN), including the control topology of Fig. 8, is implemented using a low-cost 16-b fixed-point DSP (DSPIC30F family from Microchip). The only analog component used to implement the antialiasing is a low-pass filter. Hall-effect current sensors are used to measure the machine phase currents. A voltage transducer is used to measure the load voltage. In order to simplify the current control loop, a hysteresis current controller is implemented. However, the proposed method can also be used in PWM current controlled systems. The rotor position estimator proposed in this paper has been tested using an experimental prototype with an 8/6 SRG of 2.5 kW, $L_a \approx 50$ mH, and $L_u = 12$ mH, fed by a power inverter with six IGBT power devices and diodes, as shown in Fig. 7.

The performance of the inductance estimator with the machine operating at ≈ 880 rpm is shown in Fig. 11. For this graphic, the waveforms presented are obtained for several current demands applied to the same SRG phase. This test has been realized for both motoring and generating operations using a constant current demand for each waveform.

In Fig. 11, the dashed line indicates the unsaturated inductance measured by an RCL meter from Fluke. For training the NN, experimental data are used considering phase currents

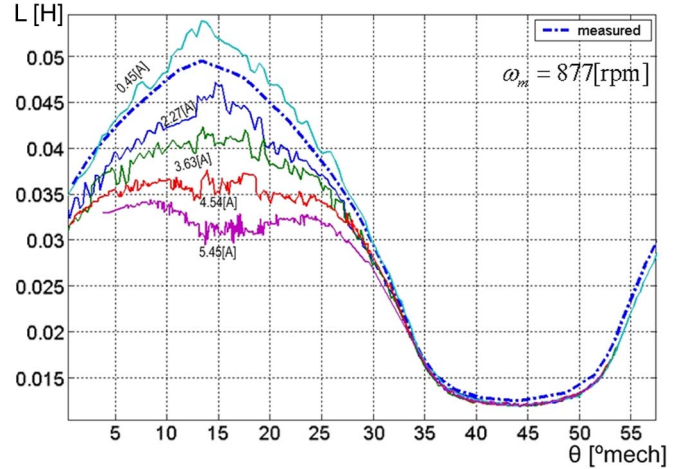


Fig. 11. Experimental comparison between the inductances measured and estimated at constant speed for different currents.

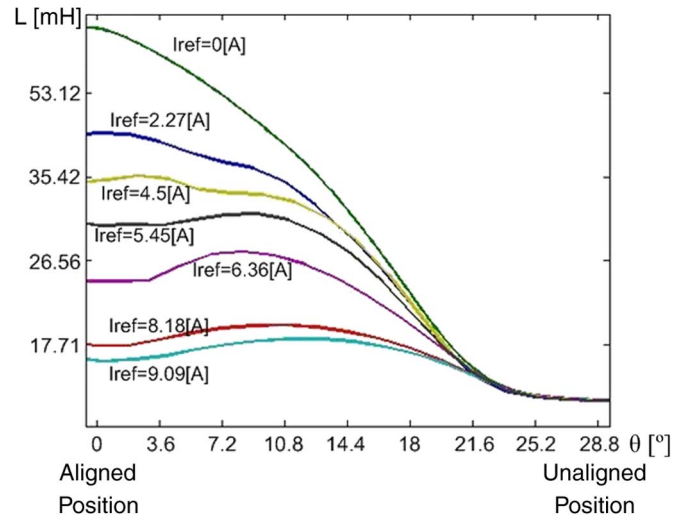


Fig. 12. Unsaturated ($I_{\text{ref}} = 0$) and estimated inductance for various phase currents.

between 5.45 and 10 A and the backpropagation algorithm. The experimental data are previously filtered using Fourier interpolation techniques. The results are shown in Fig. 12.

Using the topology of Fig. 7 and a total of 600 training samples, an average quadratic error of 3.7×10^{-4} in 1650 epochs is obtained. Only inductance curves of four phase currents from 5.45 to 10 A are used for the training process ($i = 5.45, 6.36, 8.18,$ and 10 A). No adjustment was required for lower currents, since the NN does not need to operate at low currents.

In addition, as only a good estimation of the inductance, in proximity to the unaligned position, is important, each inductance curve is considered from the local maximum toward the left. This avoids the introduction of ambiguous data in the NN. Fig. 13 shows a comparison between the curve of unsaturated inductance and the adjustment obtained with the trained NN, for four phase currents. In general, the NN fits very well to the real inductance, although, for certain positions, the error increases slightly (see $I = 8.18$ A in Fig. 13). Nevertheless, that region is

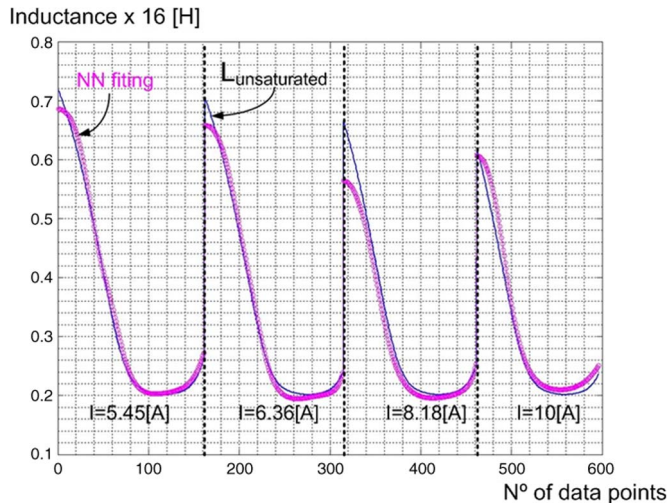


Fig. 13. Comparison between unsaturated inductance and the NN curve.

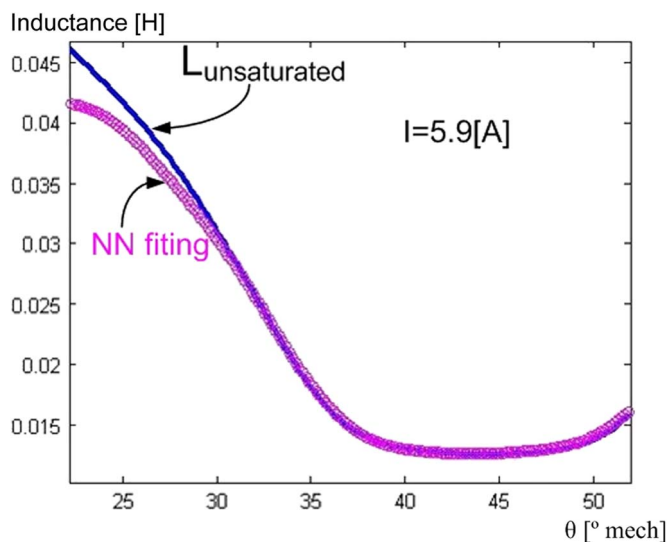


Fig. 14. Adjustment of the NN for nontrained data.

close to the aligned position ($L > 31$ mH) and is not important for the correct operation of the proposed sensorless method.

Fig. 14 shows the adjustment of the NN to a phase current waveform for which the NN has not been trained. The NN is able to interpolate the data correctly.

A. Implementation and Test of the Controller and NN

The implementation of the activation function, $\tanh()$, is realized in a lookup table of 256 values. The intermediate data are calculated by linear interpolation.

The LMS and the NN algorithm require a total of 260 CPU instructions ($8.8 \mu\text{s}$ at 29 MIPS). The sampling frequency of the ADC for the phase currents is 81 920 kcps. The nonlinear function that determines the demanded voltage is implemented in a lookup table of 27 values.

In Figs. 15 and 16, an experimental test of the SRG, subject to changes in the rotor speed, is shown, demonstrating the feasibility of the proposed sensorless control system to regulate

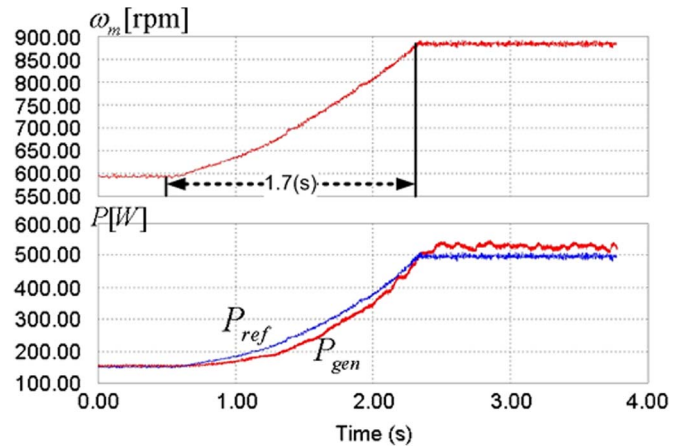


Fig. 15. Power generated in a Ramp acceleration from 600 to 880 rpm in 1.7 s.

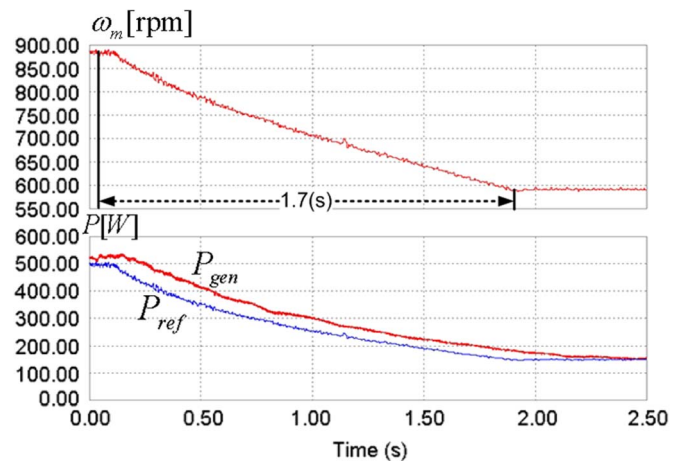


Fig. 16. Power generated in a Ramp deceleration from 880 to 600 rpm in 1.7 s.

TABLE I
SUMMARY OF ACCELERATION AND DECELERATION VALUES FOR A WIND TURBINE OF 2.5 kW UNDER TWO WIND PROFILES

	Mean turbulence intensity	Average acceleration/deceleration on rotor speed	Maximum acc./dec.
W. p. 1	28%	31[rpm/s]	157[rpm/s]
W. p. 2	12%	17[rpm/s]	104[rpm/s]

the SRG phase currents, even when relatively fast speed variations are produced because of, for instance, high wind speed variability. For this test, the maximum speed variability is about 165 rpm/s, which is a relatively large value considering that wind turbines are high inertia machines. For instance, a small WECS with a total inertia of $0.8 \text{ kg} \cdot \text{m}^2$ [26], operating with a high-turbulence-wind regime, has a maximum $d\omega/dt$ of less than 160 rpm/s with an average acceleration value of about 30 rpm/s. These values are shown in Table I, where simulation results corresponding to a small WECS, operating with high turbulence wind profiles, are shown.

In Figs. 15 and 16, P_{ref} is the power demanded to the SRG considering the actual speed, with $k_{\text{opt}} = 6.17 \times 10^{-4}$. The maximum tracking power error is approximately 50 W,

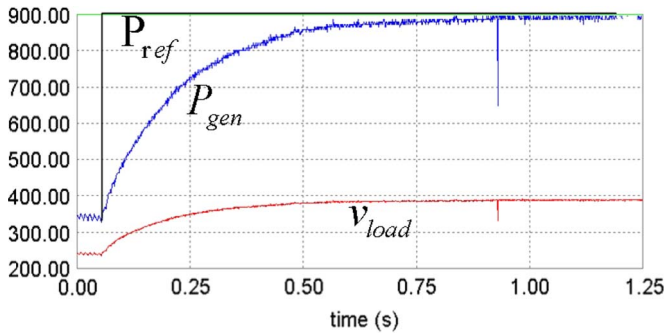


Fig. 17. Step change in power demanded, preferably in kilowatts.

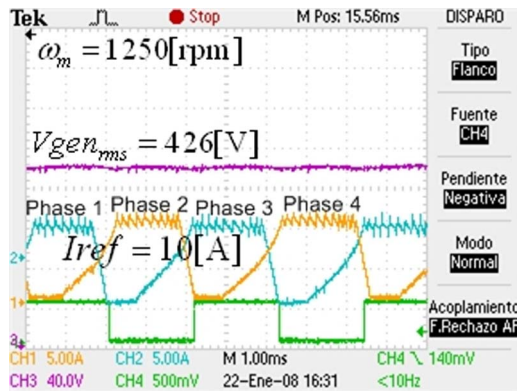


Fig. 18. Experimental waveforms of phase current, generated voltage, and pulse train from encoder.

considering a maximum acceleration or deceleration of 165 rpm/s.

In Fig. 17 a step change in P_{ref} from 350 to 900 [W] is presented. The PI controller regulates the generated voltage (v_{load}) producing a smooth and stable response with a settling time of about 0.9 (s). In Fig. 18 the phase currents and the generated voltage are presented. The pulse train is a signal derived from the encoder that indicates the unaligned positions for every phase, i.e., the instant where the phase current must reach zero.

Fig. 19 shows the voltage and current waveforms and the unaligned position pulse when the maximum error is obtained at the moment when current is extinguished. In angle terms it corresponds to an error of 1.93° (mechanical degrees), since the pulse is 15° wide. Nevertheless, this position error does not have any considerable effect in the proposed control system. Fig. 20 presents a comparison when the NN is active and inactive. It is observed clearly that the delay error is greater when NN is inactive.

VII. CONCLUSION

A new method for sensorless control of a variable speed SRG has been proposed. The scheme is suitable for a WECS. The rotor position evaluation is based on the estimation of the instantaneous inductance of the machine. The proposed approach is different from classic sensorless methods because the signal processing created in the NN is simpler. Most of

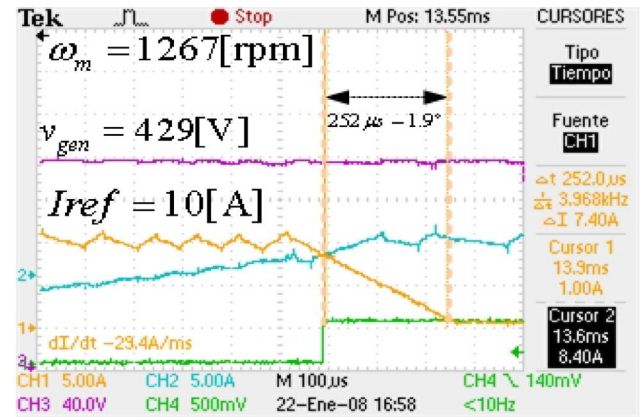


Fig. 19. Maximum delay between the extinguished current and the pulse of the unaligned position.

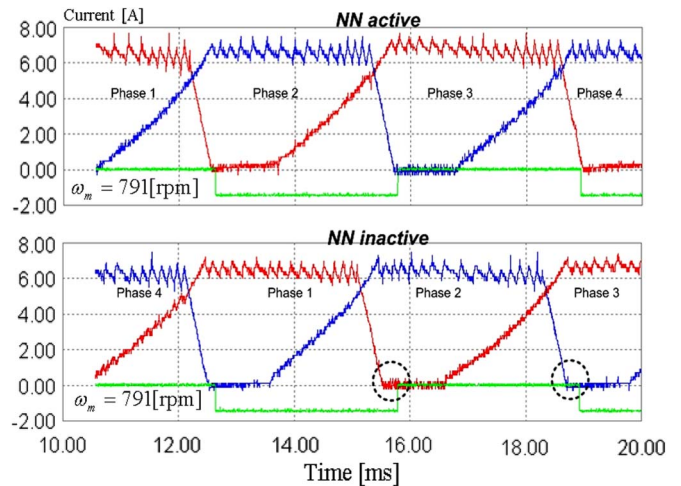


Fig. 20. Comparison when the NN is activated and deactivated.

the processing effort is generated by the LMS algorithm. For that reason the NN requires only a few neurons, reducing remarkably the processing time. In addition, there is no need of analog integrators as it is the case of the methods based in flux linkage estimation. The proposed sensorless method is not affected by variations in the phase resistance and consequently can operate at very low speed. It is applicable to a wide range of mechanical speeds (from standstill to medium speeds) and can be completely implemented in a single low cost processor. The proposed method is not suitable for single pulse control, because of resolution problems. However, sensorless methods for single-pulse control are well developed and can complement the method proposed in this work.

REFERENCES

- [1] M. A. Mueller, "Design and performance of a 20 kW, 100 rpm, switched reluctance generator for a direct drive wind energy converter," in *Proc. IEEE Int. Conf. Elect. Mach. Drives*, Mar. 2005, pp. 56–63.
- [2] R. Cardenas, R. Pena, M. Perez, J. Clare, G. Asher, and P. Wheeler, "Control of a switched reluctance generator for variable-speed wind energy applications," *IEEE Trans. Energy Convers.*, vol. 20, no. 4, pp. 781–791, Dec. 2005.

- [3] K. Ogawa, N. Yamamura, and M. Ishida, "Study for small size wind power generating system using switched reluctance generator," in *Proc. IEEE ICIT*, Dec. 2006, pp. 1510–1515.
- [4] A. Fleury, D. A. De Andrade, D. S. E. S. Felipe, and J. L. Domingos, "Switched reluctance generator for complementary wind power generation in grid connection," in *Proc. IEMDC-IEEE*, May 2007, pp. 465–470.
- [5] P. Asadi, M. Ehsani, and B. Fahimi, "Design and control characterization of switched reluctance generator for maximum output power," in *Proc. 21st Annu. IEEE APEC*, Mar. 2006, pp. 1639–1644.
- [6] C. Mademlis and I. Kioskeridis, "Optimizing performance in current-controlled switched reluctance generators," *IEEE Trans. Energy Convers.*, vol. 20, no. 3, pp. 556–565, Sep. 2005.
- [7] R. G. Lopez and B. Diong, "Simplified control of switched reluctance machines for AC generation," in *Conf. Rec. IEEE IAS Annu. Meeting*, Oct. 2004, vol. 1, p. 409.
- [8] N. Radimov, N. Ben-Hail, and R. Rabinovici, "Switched reluctance machines as three-phase AC autonomous generator," *IEEE Trans. Magn.*, vol. 42, no. 11, pp. 3760–3764, Nov. 2006.
- [9] R. Cardenas, R. Pena, M. Perez, J. Clare, G. Asher, and P. Wheeler, "Power smoothing using a flywheel driven by a switched reluctance machine," *IEEE Trans. Ind. Electron.*, vol. 3, no. 4, pp. 1086–1093, Jun. 2006.
- [10] M. Ehsani and B. Fahimi, "Elimination of position sensors in switched reluctance motor drives: State of the art and future trends," *IEEE Trans. Ind. Electron.*, vol. 49, no. 1, pp. 40–47, Feb. 2002.
- [11] P. Vas, *Artificial-Intelligence-Based Electrical Machines and Drives: Application of Fuzzy, Neural, Fuzzy-Neural, and Genetic-Algorithm-Based Techniques*. London, U.K.: Oxford Univ. Press, 1999.
- [12] E. Mese and D. A. Torrey, "An approach for sensorless position estimation for switched reluctance motors using artificial neural networks," *IEEE Trans. Power Electron.*, vol. 17, no. 1, pp. 66–75, Jan. 2002.
- [13] S. Paramasivam, S. Vijayan, M. Vasudevan, R. Arumugam, and R. Krishnan, "Real-time verification of AI based rotor position estimation techniques for a 6/4 pole switched reluctance motor drive," *IEEE Trans. Magn.*, vol. 43, no. 7, pp. 3209–3222, Jul. 2007.
- [14] C. A. Hudson, N. S. Lobo, and R. Krishnan, "Sensorless control of single switch-based switched reluctance motor drive using neural network," *IEEE Trans. Ind. Electron.*, vol. 55, no. 1, pp. 321–329, Jan. 2008.
- [15] T. Liu and C. Chen, "Implementation of a sensorless switched reluctance drive with self-inductance estimating technique," in *Proc. 28th Annu. Conf. IEEE Ind. Electron. Soc.*, Nov. 2002, pp. 508–513.
- [16] I. H. Al-Bahadly, "Examination of a sensorless rotor-position-measurement method for switched reluctance drive," *IEEE Trans. Ind. Electron.*, vol. 55, no. 1, pp. 288–295, Jan. 2008.
- [17] D. Panda and V. Ramanarayanan, "Reduced acoustic noise variable DC-bus-voltage-based sensorless switched reluctance motor drive for HVAC applications," *IEEE Trans. Ind. Electron.*, vol. 54, no. 4, pp. 2065–2078, Aug. 2007.
- [18] A. Khalil, S. Underwood, I. Husain, H. Klode, B. Lequesne, S. Gopalakrishnan, and A. M. Omekanda, "Four-quadrant pulse injection and sliding-mode-observer-based sensorless operation of a switched reluctance machine over entire speed range including zero speed," *IEEE Trans. Ind. Appl.*, vol. 43, no. 3, pp. 714–723, May/Jun. 2007.
- [19] C. S. Edrington, R. B. Sepe, Jr., and B. Fahimi, "Sensorless super-high-speed switched reluctance generators," in *Proc. 28th Annu. Conf. IEEE Ind. Electron. Soc.*, Nov. 2002, pp. 1026–1031.
- [20] S. R. Jones and B. T. Drager, "Sensorless switched reluctance starter/generator performance," *IEEE Ind. Appl. Mag.*, vol. 3, no. 6, pp. 33–38, Nov./Dec. 1997.
- [21] J. W. Dixon, M. Rodríguez, and R. Huerta, "Position estimator and simplified current control strategy for brushless-DC motors, using DSP technology," in *Proc. IEEE IECON*, Nov. 2002, pp. 590–596, CD-ROM.
- [22] B. K. Bose, "Neural network applications in power electronics and motor drives—An introduction and perspective," *IEEE Trans. Ind. Electron.*, vol. 54, no. 1, pp. 14–33, Feb. 2007.
- [23] I. Husain and M. Ehsani, "Torque ripple minimization in switched reluctance motor drives by PWM current control," *IEEE Trans. Power Electron.*, vol. 11, no. 1, pp. 83–88, Jan. 1996.
- [24] I. Husain, "Minimization of torque ripple in SRM drives," *IEEE Trans. Ind. Electron.*, vol. 49, no. 1, pp. 28–39, Feb. 2002.
- [25] D. A. Torrey, "Switched reluctance generators and their control," *IEEE Trans. Ind. Electron.*, vol. 49, no. 1, pp. 3–14, Feb. 2002.
- [26] R. Cárdenas, "Control of a switched reluctance generator for wind energy applications." Ph.D. dissertation, School Elect. Electron. Eng., Univ. Nottingham, Nottingham, U.K., Jun. 1996.



Estanislao Echenique was born in Rancagua, Chile. He received the B.S. and M.Sc. degrees in electrical engineering from the Pontificia Universidad Católica de Chile, Santiago, Chile, in 2008.

From 2006 to 2008, he was a Student Researcher with the "Núcleo de Electrónica Industrial y Mecatrónica," Santiago. He is currently a Consulting Engineer with Systep Engineering and Design Company. He has worked on research projects on power electronics, electric vehicles with PV cells, and antiseismic instrumentation. His main interests

include power electronics and machine control for renewable energy.



Juan Dixon (M'90–SM'95) was born in Santiago, Chile. He received the B.S. degree in electrical engineering from the Universidad de Chile, Santiago, in 1977, and the M.Eng. and Ph.D. degrees from McGill University, Montreal, QC, Canada, in 1986 and 1988, respectively.

In 1976, he was with the State Transportation Company in charge of trolleybus operations. In 1977 and 1978, he was the Chilean Railways Company. Since 1979, he has been with the Department of Electrical Engineering, Pontificia Universidad Católica de Chile, Santiago, where he is currently a Professor. He has presented more than 70 works at international conferences and has published around 40 papers related to power electronics in *IEEE TRANSACTIONS* and *IEE Proceedings*. His main areas of interest include electric traction, power converters, pulsewidth-modulation rectifiers, active power filters, power factor compensators, and multilevel and multistage converters. He has conducted consulting work related to trolleybuses, traction substations, machine drives, hybrid electric vehicles, and electric railways. He has created an Electric Vehicle Laboratory, where he has built state-of-the-art vehicles using brushless dc machines with ultracapacitors and high specific energy batteries.



Roberto Cárdenas (S'95–M'97–SM'07) was born in Punta Arenas, Chile. He received the Electrical Engineering degree from the University of Magallanes, Punta Arenas, in 1988, and the M.Sc. and Ph.D. degrees from the University of Nottingham, Nottingham, U.K., in 1992 and 1996, respectively.

From 1989 to 1991, he was a Lecturer with the University of Magallanes. From 1992 to 1996, he was with the PMC Group, University of Nottingham.

He is currently with the Department of Electrical Engineering, Universidad de Magallanes. His main interests include the control of electrical machines, variable-speed drives, and renewable energy systems. He was appointed Professor of Electrical Drives in 2006.

Prof. Cárdenas received the Best Paper Award of the *IEEE TRANSACTIONS ON INDUSTRIAL ELECTRONICS* in 2005.



Ruben Peña (S'95–M'97) was born in Coronel, Chile. He received the Electrical Engineering degree from the University of Concepción, Concepción, Chile, in 1984, and the M.Sc. and Ph.D. degrees in electrical engineering from the University of Nottingham, Nottingham, U.K., in 1992 and 1996, respectively.

He is currently with the Department of Electrical Engineering, Universidad de Concepción. His current research interests include the control of power electronic converters, ac drives, and renewable energy systems.